Electronic and Vibrational Structures of Corannulene Anions

Tohru Sato,* Atsushi Yamamoto, and Tokio Yamabe

Department of Molecular Engineering, Graduate School of Engineering, Kyoto University, Sakyo-ku, Kyoto 606-8501, Japan

Received: August 18, 1999; In Final Form: October 12, 1999

Electronic and vibrational structures of anionic corannulenes, $C_{20}H_{10}^{-}$, $C_{20}H_{10}^{2-}$, $C_{20}H_{10}^{3-}$, and $C_{20}H_{10}^{4-}$, are studied on the basis of the ab initio molecular orbital calculation at the HF/6-31G**, MP2/6-31G**//HF/6-31G**, and CASSCF/6-31G**//HF/6-31G** levels of theory. Analytical solutions of Hückel Hamiltonian are also presented. The difference in geometries and electronic and vibrational structures among these corannulene anions, and the Jahn−Teller effect appearing in $C_{20}H_{10}^{-}$ and $C_{20}H_{10}^{3-}$ are discussed. The ground state of dianion is a singlet state. It is found that the wavenumbers of the infrared-active C−H stretching mode of corannulene anions decrease linearly as corannulene become more negative. It can be used as the identification of the reduction stage of a corannulene anion. We also found that the Jahn−Teller coupling of trianion is larger than that of monoanion.

1. Introduction

A nonalternant hydrocarbon corannulene **1**, $C_{20}H_{10}$, dibenzo[*ghi*,*mno*] fluoranthene, shown in Figure 1, was first synthesized by Barth and Lawton in 1966.[1,2] Right after this synthesis it has been predicted that corannulene should show as a π-electron system an aromatic character on the basis of the self-consistent field molecular orbital (SCF-MO) calculation.[3] Corannulene has a unique bowl-shaped structure with a five-fold axis and, moreover, three corannulene skeletons can essentially construct a soccer-ball like structure.[4] It is well-known that, from this fact, Osawa has proposed in association with superaromaticity a soccer-ball like structure consisting of 60 carbon atoms fifteen years[5] before the experimental discovery of buckminsterfullerene C_{60}.[6] Since the actual discovery of fullerenes, this bowl-shaped corannulene molecule has been attracting more attention in association with organic synthesis of C_{60} as well as chemistry of corannulene itself.

A new and convenient synthetic method of corannulene using flash vacuum pyrolysis technique has recently been developed,[7−9] which has accelerated experimental studies on corannulene and some interesting findings have been issued. One of these is that this hydrocarbon is a very flexible aromatic compound capable of performing bowl-to-bowl inversion as has been predicted,[10] the barrier of which has been experimentally estimated to be $\Delta G^{\ddagger} = 10.2 + 0.2$ kcal/mol for a corannulene ring system.[11]

The lowest unoccupied molecular orbitals (LUMO) of corannulene are rather low-lying and doubly degenerate,[12,13] which signifies that the reduced states of corannulene could be possibly stable even in highly anionized state. This is similar to C_{60}, which has a three-fold degenerate LUMOs and can accept six extra electrons to form higher anions. In fact, all of the anionic species from mono- to tetraanion have been observed.[12,14,15] For instance, a corannulene monoanion radical has been electrochemically prepared and observed using the electron spin resonance (ESR) technique.[14] Moreover, higher (di-, tri-, and tetra-) anions have been prepared with alkali-metal (Li or K) reduction and examined using optical absorption, ESR, and nuclear magnetic resonance (NMR) spectroscopy.[12,15] Both NMR and ESR spectroscopy have shown that dianion is diamagnetic. Semiempirical calculation (AM1) has also shown that the ground state of dianion is a singlet state. Barth and Lawton visualized that neutral corannulene can be thought of an "annulene within an annulene": aromatic hub carbons has 6e/5C and aromatic rim carbons has 14e/15C. In other words, corannulene is thought to consist of cyclopentadienyl ([5]-annulene) anion and [15]annulene cation. They have concluded that because of 16e on the rim carbons in dianion large paratropic ring current strongly shields the peripheral hydrogen atoms and strongly deshields the inner carbons. The singlet−triplet energy difference was evaluated to be 0.24 eV, which suggests that there exists a low-lying triplet state. The reduction to trianion and tetraanion can be achieved only with lithium metal. Potassium cannot reduce to higher stage than trianion. For both the dianionic and trianionic states corannulene dimer cannot observed, whereas dimer form has been observed in the tetraanion solution.[16] In tetrahydrofuran solution, two corannulene tetraanion forms a sandwich compound which has 10 components: it contains four lithium cations inside and four outside.[16]

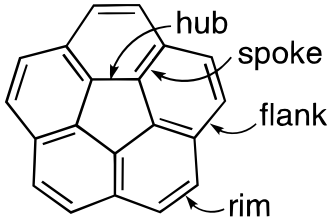

Figure 1. The structure of corannulene, $C_{20}H_{10}$, dibenzo[*ghi*,*mno*] fluoranthene. There are four types of C−C bonds, hub, spoke, flank, and rim.

Kiyobayashi et al. have measured the standard formation enthalpy of corannulene by microbomb combustion calorimetry.[17] They estimated the standard formation enthalpy in gas phase to be 463.7 kcal·mol^{-1}. Structural and heat-of-formation analyses of the neutral corannulene **1** by the ab initio MO calculation have been established,[18] as well as the estimation

* To whom correspondence should be addressed.

10.1021/jp992912x CCC: $19.00
Published on Web 12/14/1999

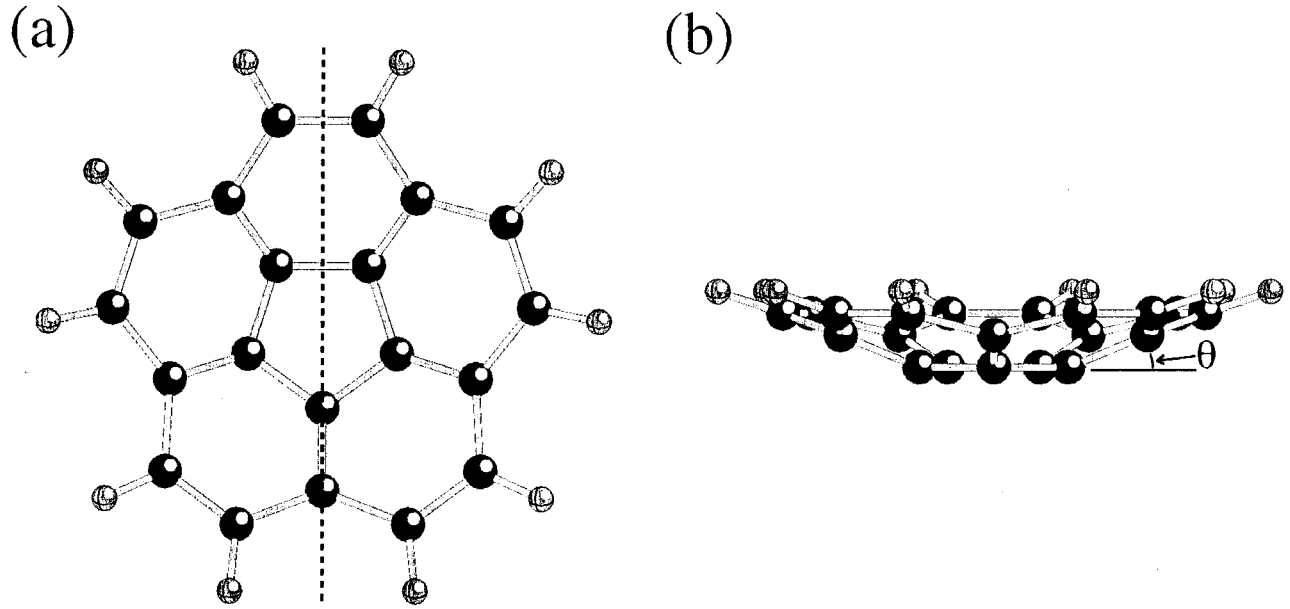

Figure 2. The bowl-shaped structure of corannulene. (a) topview and (b) sideview, respectively. The broken line in (a) represents the mirror plane of the symmetry element in C_s group and θ in (b) indicates a "bowl angle" (see text).

of its inversion barrier at the semiempirical (AM1) MO and the local density functional method levels.[8] The ab initio studies on $\mathbf{1}^-$,[19] $\mathbf{1}^{2-}$,[20] and $\mathbf{1}^{4-}$ [20,21] have been published.

In the present study we report the electronic and vibrational structure analysis of corannulene anions, $\mathbf{1}^{n-}$ (n = 0, 1, 2, 3, and 4), on the basis of ab initio MO calculations in the Hartree−Fock approximation as well as the post Hartree−Fock theories. This species is of interest in that Jahn−Teller (JT) distortion should occur at the monoanionic and trianionic states, which could afford some comparison with the anionic state of C_{60}[22,23] as well.

2. Analytical Solutions of Hückel Hamiltonian

Prior to extensive calculations, we present analytical solutions of the secular equation within the Hückel approximation.

Using point group C_{5v}, the reducible representation constructed by π orbital is reduced as

$$\Gamma_{\pi\mathrm{MO}} = 3\mathrm{a}_1 + \mathrm{a}_2 + 4\mathrm{e}_1 + 4\mathrm{e}_2 \tag{1}$$

As pointed out later, there occurs symmetry-lowering, $C_{5v} \rightarrow C_s$, in anionic states, because of the JT or pseudo JT distortions. The compatibility relations between C_{5v} and C_s is

$$\mathrm{a}_1 \downarrow C_s = \mathrm{a}', \mathrm{a}_2 \downarrow C_s = \mathrm{a}'', \mathrm{e}_1 \downarrow C_s = \mathrm{a}' + \mathrm{a}'', \quad \mathrm{e}_2 \downarrow C_s = \mathrm{a}' + \mathrm{a}'' \tag{2}$$

The secular equation of the Hückel Hamiltonian is factorized into the following four equations:

$$x + 1 = 0 \tag{3}$$

$$x_3 - 3x^2 - x + 5 = 0 \tag{4}$$

$$\left(x^4 - \frac{\sqrt{5}-1}{2}x^3 - 4x^2 + (\sqrt{5}-1)x - \frac{\sqrt{5}-5}{2}\right)^2 = 0 \tag{5}$$

$$\left(x^4 + \frac{\sqrt{5}+1}{2}x^3 - 4x^2 - (\sqrt{5}+1)x + \frac{\sqrt{5}+5}{2}\right)^2 = 0 \tag{6}$$

From eq 3 it is clear that $x = -1$ is one of the solutions. This eigenvalue belongs to a_2 representation. Solutions of eq 4 are expressed by

$$x = 1 + \frac{4}{\sqrt{3}}\cos\left(\frac{1}{3}(\pi - \alpha)\right) \tag{7}$$

$$1 - \frac{2}{\sqrt{3}}\cos\left(\frac{1}{3}(\pi - \alpha)\right) + \frac{2}{\sqrt{3}}\sin\left(\frac{1}{3}(\pi - \alpha)\right) \tag{8}$$

$$1 - \frac{2}{\sqrt{3}}\cos\left(\frac{1}{3}(\pi - \alpha)\right) - \frac{2}{\sqrt{3}}\sin\left(\frac{1}{3}(\pi - \alpha)\right) \tag{9}$$

where $\tan\alpha = \sqrt{37/27}$. These belong to a_1 representation. Since eqs 5 and 6 are squares of a biquadratic expression, the remaining 16 solutions make a pair, each of which belongs twofold degenerate representations e_1 and e_2, respectively. The remaining solutions are given by the two biquadratic equations—eqs 5 and 6. Equation 5 gives

$$x = \frac{-1 + \sqrt{11 \pm 2\sqrt{5}}}{2} \tag{10}$$

$$\frac{1+\sqrt{5}}{4} \pm \sqrt{\frac{11+\sqrt{5}}{8}} \tag{11}$$

Equation 6 is solved as

$$x = \frac{1-\sqrt{5}}{4} \pm \sqrt{\frac{11-\sqrt{5}}{8}} \tag{12}$$

$$\frac{-1 - \sqrt{11 \pm 2\sqrt{5}}}{2} \tag{13}$$

The MO patterns near the frontier level and the approximate eigenvalues as well as the analytical ones are shown in Figure 3 and Table 1, respectively.

Since the LUMOs are degenerate, there are some (more than two) electronic states in mono-, di-, and trianionic states, and charge-induced JT distortion should occur in the case of mono- and trianionic states owning to the Jahn−Teller theorem.[24] For monoanion, the additional electron occupies one of the LUMOs,

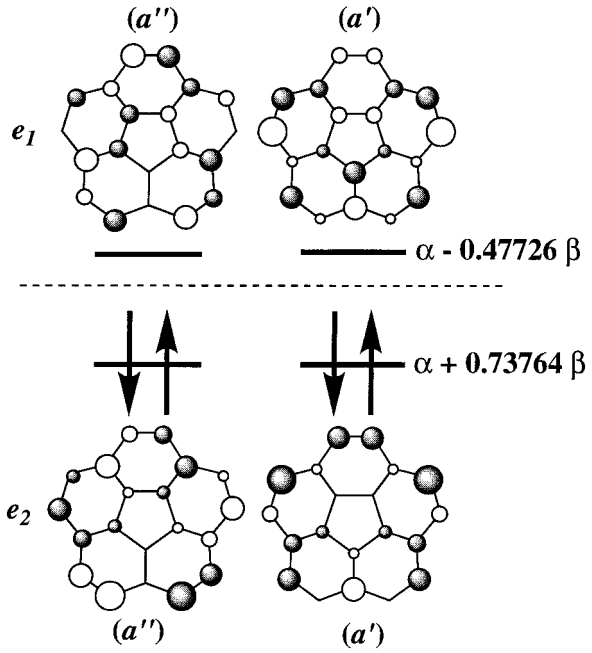

Figure 3. The Hückel molecular orbitals (MO) of corannulene. The highest occupied MO (HOMO) is e_2 state, and the lowest unoccupied MO (LUMO) is e_1 state. The symmetry species in the parentheses denote the compatibility relation between C_{5v} and C_s.

that is a′ or a″ state with the symmetry lowering. In the former case, the electronic state is ^{2}A′ and the latter is ^{2}A″. Trianion is the same as monoanion: ^{2}A′ and ^{2}A″ state can be considered. In such JT systems, one should be a minimum, and the other a saddle point of adiabatic potential. For dianion, there are three ways for the two extra electrons to occupy the LUMOs partially. When two electrons completely fill one orbital, either a′ or a″, the term is ^{1}A′ state, In addition, triplet state appears if each of LUMOs is singly occupied by one electron with the same spin. It is interesting whether the ground state of dianion is triplet or singlet. Moreover, pseudo JT distortion may occur in dianion and tetraanion because of rather low-lying LUMO+1 or LUMO+2. To address these problems, we will go into quantitative ab initio MO calculations in the next section.

3. Ab Initio Calculation

3.1. Method of Calculation. Radom has reviewed computational studies on various molecular anions including only first-row elements.[25] He has concluded that reliable structural predictions may be made from single-determinant molecular orbital calculations with double-ζ basis sets though electron affinity is not reliable. We employed Hartree−Fock (HF) method for the geometry optimizations of the anions. Therefore we will not discuss electron affinities here. Furthermore, we applied second-order Møller−Plesset (MP2) perturbation theory and complete active space self-consistent field (CASSCF) theory for the optimized geometries with Hartree−Fock calculations to estimate the correlation energy. Polarization function is important to obtain reliable bond angles.[26] Hence, we used 6-31G** basis set for both carbon and hydrogen. We also tried to add diffuse functions, since it is desirable to calculate such anionic systems. However, we could not obtain any self-consistent field for the present systems. The Gaussian 94 program[27] and Gaussian 98 program[28] on CRAY T94 and Origin2000 have been employed for carrying out both the HF MO calculations and post HF calculations, based on the gradient-optimized geometry. Restricted Hartree−Fock method (RHF) were applied for the optimizations of the closed shell species, neutral **1**, singlet states of dianion $\mathbf{1}^{2-}$, and tetraanion $\mathbf{1}^{4-}$. On the other hand, for the optimizations of the open shell systems, monoanion $\mathbf{1}^{-}$, triplet state of dianion $\mathbf{1}^{2-}$, and trianion $\mathbf{1}^{3-}$, unrestricted Hartree−Fock (UHF) method were employed. After each species was optimized at the HF level of theory, a single-point MP2 calculation was performed on the geometry. Furthermore we applied CASSCF theory for optimized geometries with HF method. We chose the active space spanned by four and six orbitals with five electrons (CAS(5,4) and CAS(5,6)) for $\mathbf{1}^{-}$, four and six orbitals with six electrons (CAS(6,4) and CAS(6,6)) for $\mathbf{1}^{2-}$, and three and four orbitals with three electrons (CAS(3,3) and CAS(3,4)) for $\mathbf{1}^{3-}$, respectively.

In the process of geometrical optimization the symmetries of $\mathbf{1}^{-}$, $\mathbf{1}^{2-}$, $\mathbf{1}^{3-}$, and $\mathbf{1}^{4-}$ were kept to be C_s or C_1 symmetry being plausible after the Jahn−Teller distortion, where the mirror plane is shown in Figure 2a. The geometry of **1** was fixed to have C_{5v} symmetry as has been reported.[18,21] To evaluate the magnitude of JT stabilization energies for $\mathbf{1}^{-}$ and $\mathbf{1}^{3-}$ we also tried optimization of the geometries with C_{5v} symmetry for them.

TABLE 1. Analytical Expressions and Approximate Values of Hückel Molecular Orbital Energy: The Unit Is the Resonance Energy β[a]

orbital	analytical expression/β	approximate value/β
$a_1(1)$	$1+\frac{4}{\sqrt{3}}\cos\left(\frac{1}{3}(\pi-\alpha)\right)$	2.67513
$e_1(1)$	$\frac{1+\sqrt{5}}{4}+\sqrt{\frac{11+\sqrt{5}}{8}}$	2.09529
$a_1(2)$	$1-\frac{2}{\sqrt{3}}\cos\left(\frac{1}{3}(\pi-\alpha)\right)+\frac{2}{\sqrt{3}}\sin\left(\frac{1}{3}(\pi-\alpha)\right)$	1.53919
$e_2(1)$	$\frac{-1+\sqrt{11+2\sqrt{5}}}{2}$	1.46673
$e_1(2)$	$\frac{-1+\sqrt{11-2\sqrt{5}}}{2}$	0.777484
e_2(2, HOMO)	$\frac{1-\sqrt{5}}{4}+\sqrt{\frac{11-\sqrt{5}}{8}}$	0.73764
e_1(3, LUMO)	$\frac{1+\sqrt{5}}{4}-\sqrt{\frac{11+\sqrt{5}}{8}}$	−0.47726
$a_2(1)$	−1	−1.00000
$a_1(3)$	$1-\frac{2}{\sqrt{3}}\cos\left(\frac{1}{3}(\pi-\alpha)\right)-\frac{2}{\sqrt{3}}\sin\left(\frac{1}{3}(\pi-\alpha)\right)$	−1.21432
$e_2(3)$	$\frac{1-\sqrt{5}}{4}-\sqrt{\frac{11-\sqrt{5}}{8}}$	−1.35567
$e_1(4)$	$\frac{-1-\sqrt{11-2\sqrt{5}}}{2}$	−1.77748
$e_2(4)$	$\frac{-1-\sqrt{11+2\sqrt{5}}}{2}$	−2.46673

[a] Where $\tan\alpha=\sqrt{37/27}$.

TABLE 2: HF/6-31G Optimized Bond Lengths/angstroms and Bowl Angles/degree (See Text) of the Ground States of Corannulene Anions[a]**

		hub	spoke	flank
1	$^1A_1$	1.412 (1.413)	1.361 (1.391)	1.450 (1.440)
$\mathbf{1}^-$	$^2A''$	1.385−1.440	1.392−1.402	1.409−1.466
$\mathbf{1}^{2-}$	$^1A'$	1.368−1.423	1.392−1.414	1.380−1.482
$\mathbf{1}^{3-}$	$^2A'$	1.386−1.403	1.410−1.421	1.409−1.445
$\mathbf{1}^{4-}$	$^1A'$	1.391−1.400	1.435−1.444	1.375−1.487

	rim	C−H	bowl angle
1	1.3780 (1.402)	1.077 (1.01)	21.17 (22.4)
$\mathbf{1}^-$	1.397−1.434	1.079−1.080	19.79−21.31
$\mathbf{1}^{2-}$	1.361−1.455	1.082−1.086	17.48−19.87
$\mathbf{1}^{3-}$	1.455−1.472	1.088−1.090	15.16−15.59
$\mathbf{1}^{4-}$	1.403−1.520	1.094−1.100	12.81−17.13

[a] Experimental values[4] are in the parentheses.

We adopt the C_{5v} structures giving their lowest energy. Except for the C_{5v} structure of $\mathbf{1}^-$ and $\mathbf{1}^{3-}$, each optimized structure thus obtained was confirmed to be a minimum, that is, to have the Hessian matrix with positive definite eigenvalues by using the vibrational analysis. All the frequencies presented here are scaled by a factor, 0.8929.[29]

3.2. Optimized Geometries. The optimized bond lengths of the ground state of $\mathbf{1}^{n-}$ (n = 0, 1, 2, 3, and 4) at HF/6-31G** level are given in Table 2. The symmetry of the optimized structure of neutral **1** is C_{5v}. This structure indicates bond alternation as shown in Figure 1. From the bond lengths, spoke and rim have a double-bond nature, while hub and flank are a single bond. The structures of all the other anions have C_s symmetry. These symmetry lowering from C_{5v} to C_s are due to JT or pseudo JT effect in these systems. The symmetry-broken geometries of the dianion and the tetraanion have been obtained by Sygula and Rabideau also.[20]

On the whole, as shown in Table 2, as the system accepts more electrons the lengths of spoke, rim, and C−H bond of the anion become longer. This is because the antibonding nature at spoke and rim of LUMOs, shown in Figure 3, and electron localization on the peripheral carbons. The localized electron on the rims give rise to increase C−H bond length as well as that of rim. To compare the curvature among corannulene anions, angles between a spoke and the basal plane defined by two hubs connecting the spoke, which is called "bowl angles" throughout this paper, are listed in Table 2. The bowl angles of the anions seem to become smaller, in other words, flatter as the reduction proceeds. Contrary to our previous work,[19] the optimized structure of $\mathbf{1}^{4-}$ is still bowl shaped, the bowl angle of which is in the range of 12.81°−17.13°. This is the effect of polarization function in the basis functions. The preference for bowl-shaped structures of the dianion and the tetraanion has been also reported.[20]

3.3. Energetics. Total energies of the ground state of **1**, $\mathbf{1}^-$, $\mathbf{1}^{2-}$, $\mathbf{1}^{3-}$, and $\mathbf{1}^{4-}$ and relative energy of other states with respect to the ground state are tabulated in Tables 3 and 4, respectively.

The HF and MP2 calculations show that the ground state of the monoanion is $^2A'$, which lies below the $^2A''$ state by ca. 0.02 eV and 0.29 eV, respectively. However, the CASSCF calculations of $\mathbf{1}^-$ indicate the opposite result. Including electron correlation by CASSCF method, the ground state of monoanion at the HF optimized geometry is $^2A''$.

As for $\mathbf{1}^{2-}$, the energy differences between singlet and triplet state of dianion $\mathbf{1}^{2-}$ are summarized in Table 5. All the levels of the calculations indicate that singlet state is a ground state although the relative stability of the two singlet states depends on the approximations as shown in Table 4. It has been reported that the triplet state is the ground state in the C_{5v} geometry, while the symmetry lowering make the ground state of the dianion singlet.[20] It is consistent with the experimental observation.[15] The triplet excited-state lies above the singlet states by ca. 0.2 eV from the restricted open-shell HF (ROHF) calculation.

For $\mathbf{1}^{3-}$, $^2A'$ state is a ground state in the HF/6-31G** level of calculation. However, the MP2 and CASSCF calculations indicate the opposite result. Including electron correlation, the ground state of trianion at its HF-optimized structure is $^2A''$.

3.4. Electronic Structure. The atomic net charges are shown in Table 6. Hydrogen atoms of **1** are positively charged, whereas the charges of the rim carbon atoms are negative. In the anionic species, on the other hand, such positive charge on protons are gradually reduced and the hydrogen atoms of $\mathbf{1}^{3-}$ and $\mathbf{1}^{4-}$ have completely negative charges. In each anionic state, electrons are delocalized into two part, hub and rim. In other words, the extra electrons are accepted mainly by the rim and hub carbons. The rim carbon atoms in the corannulene anions become more negative than the hub carbon atoms. This is because the LUMOs of $\mathbf{1}^0$ have large coefficients on the rim carbons as shown in Figure 3. The charge on the flank carbons are always positive even in tetraanion. Such distributions cause flat structure of anionic corannulenes since the interelectron-repulsions between the rim carbon atoms increases as the reduction stage increases, and the distances between the rim carbons become longer by the decrease of bowl-angles to avoid the repulsions.

The polarization between the outer [15]annulene and the inner [5]annulene in $\mathbf{1}^0$ is not very large. From the electronic structure and the bond-alternation pattern, neutral corannulene is not so much "annulene within annulene" as "[5]radialene with five ethylenes".

The spin density distributions of $\mathbf{1}^-$ and $\mathbf{1}^{3-}$ calculated with MP2/6-31G** level are shown in Figure 4. Comparing the signs of the spins in the mono- and trianion, almost the same alternating patterns are found except for the sign of the spin on the flank and rim carbons shown in the lower of Figure 4. In $\mathbf{1}^-$, there is a large spin polarization in five carbons on the hub and two on the spokes. In trianionic state, corannulene has a beltlike spin distribution crossing the molecule.

3.5. Vibrational Structures. There are $3N - 6 = 84$ normal modes in these systems. The irreducible representations of the normal modes are

TABLE 3: Total Energies of the Ground States of Corannulene Anions in eV

			CAS/6-31G**//HF/6-31G**	
	HF/6-31G**	MP2/6-31G**//HF/6-31G**	smaller space	larger space
1	−20767.886817	−20838.443719		
$\mathbf{1}^-$	−20767.514361	−20835.694577	−20766.882577[a]	−20767.611828[d]
$\mathbf{1}^{2-}$	−20761.681609	−20834.095233	−20762.029353[b]	−20763.010823[e]
$\mathbf{1}^{3-}$	−20753.522694	−20824.936808	−20752.953650[c]	−20753.028624[f]
$\mathbf{1}^{4-}$	−20739.965982	−20813.748974		

[a] CAS(5,4)/6-31G**//HF/6-31G**. [b] CAS(6,4)/6-31G**//HF/6-31G**. [c] CAS(3,3)/6-31G**//HF/6-31G**. [d] CAS(5,6)/6-31G**//HF/6-31G**. [e] CAS(6,6)/6-31G**//HF/6-31G**. [f] CAS(3,4)/6-31G**//HF/6-31G**.

TABLE 4: Relative Energies of Some States of 1^-, 1^{2-}, and 1^{3-} in eV with Respect to the Ground State: The Symbol [1^0] Signifies the Electronic Ground-State Configuration of Neutral Corannulene

		orbital occupation	HF/6-31G**	MP2/6-31G**// HF/6-31G**
1^-	$^2A'$	[1^0](37a′)	0.0	0.0
	$^2A''$	[1^0](30a″)	0.017650	0.289492
1^{2-}	$^1A'$	[1^0](37a′)^2	0.0	0.000386
		[1^0](30a″)^2	0.000519	0.0
	$^3A''$	[1^0](37a′)(30a″)	0.202904	1.613319
1^{3-}	$^2A'$	[1^0](37a′)(30a″)^2	0.0	0.275783
	$^2A''$	[1^0](37a′)^2(30a″)	0.436920	0.0

		orbital occupation	CAS/6-31G**// HF/6-31G**	
1^-	$^2A'$	[1^0](37a′)	0.044 621[a]	0.309 226[d]
	$^2A''$	[1^0](30a″)	0.0[a]	0.0[d]
1^{2-}	$^1A'$	[1^0](37a′)^2	0.038 217[b]	0.0[e]
		[1^0](30a″)^2	0.0[b]	0.267 710[e]
	$^3A''$	[1^0](37a′)(30a″)	0.537 696[b]	0.579 683[e]
1^{3-}	$^2A'$	[1^0](37a′)(30a″)^2	0.094 068[c]	0.065 665[f]
	$^2A''$	[1^0](37a′)^2(30a″)	0.0[c]	0.0[f]

[a] CAS(5,4)/6-31G**//HF/6-31G**. [b] CAS(6,4)/6-31G**//HF/6-31G**. [c] CAS(3,3)/6-31G**//HF/6-31G**. [d] CAS(5,6)/6-31G**//HF/6-31G**. [e] CAS(6,6)/6-31G**//HF/6-31G**. [f] CAS(3,4)/6-31G**//HF/6-31G**.

TABLE 5: Singlet−Triplet Energy Difference of 1^{2-} in eV

calculation method	$E_{triplet} - E_{singlet}$/eV
ROHF/6-31G**	0.202385
MP2/6-31G**//HF/6-31G**	1.613754
CASSCF(6,4)/6-31G**//HF/6-31G**	0.537696
CASSCF(6,6)/6-31G**//HF/6-31G**	0.579683

$$\Gamma_{vib} = 9A_1 + 7A_2 + 16E_1 + 18E_2 \quad (14)$$

The Raman-active modes are A_1, E_1, and E_2, and the IR-active modes are A_1 and E_1. The simulated Raman and IR spectra are shown in Figures 6 and 7.

For C_{60}, the pentagonal pintch mode $A_g(2)$ is one of the Raman-active modes and its location is proportional to the reduction state.[30,31] Similar pentagonal pintch mode should exist in the present system in the A_1 modes, and it may exhibit similar doping dependence to the $A_g(2)$ mode of C_{60}. Table 7 shows all vibration frequencies, IR intensities, and Raman activities of neutral corannulene for A_1 modes. The most intensive Raman-active mode is $A_1(9)$ (2997 cm^{-1}) and the next one is $A_1(7)$ (1414 cm^{-1}), then others are nearly inactive for Raman scattering. These vibrational modes are shown in Figure 5. For the reference, the pentagonal pinch mode of C_{60} is also included. $A_1(9)$ mode is symmetric C−H stretching mode, while the displacements of carbon atoms of $A_1(7)$ mode is very similar to the pentagonal pinch mode of C_{60} and its wavenumber is close to that of the pentagonal pinch of C_{60}. Corannulene anions does not keep to have C_{5v} symmetry due to JT or pseudo JT effect. Hence we cannot distinguish any A_1 vibrational mode corresponding to A_1 for $\mathbf{1}^0$ among these symmetry-lowered anions and find out any clear relationship in the simulated Raman spectra between the peak position and the reduction state.

On the other hand, a clear relationship between the peak position and the reduction state is found in the IR absorption spectra. As shown in Figure 7, absorptions in the range above 2500 cm^{-1}, attributing to C−H stretching modes, give rise to red shift with reduction. This is because the repulsion between the electron localized on the rim carbons and the negative charge of hydrogens weaken the C−H bonds.

Figure 8 shows the relationship between the most intensive peak position of them and the reduction state. Its dependency of the absorption corresponding to the C−H stretching mode on the reduction state is described by a simple expression, $3010 - 50n$ cm^{-1} for $\mathbf{1}^{n-}$. This relation can be used as an identification of the reduction state of a corannulene anion as the pentagonal pinch mode of $A_g(2)$ of C_{60}.

3.6. Jahn−Teller Effect. Since the symmetric product of the representation E_1 of LUMO is reduced as

$$[E_1^2] = A_1 + E_2 \quad (15)$$

the vibrational modes which couple to the degenerate electronic $^2E_1$ state and split the state are E_2 modes. The frequencies of the JT-active E_2 modes after scaling are listed in Table 7. The term of the ground vibronic state is $^2E_1$ with symmetry consideration.

The classical Jahn−Teller distortion is ruled by the magnitude of S defined by

$$S = \frac{|E_{JT}|}{\hbar\omega} \quad (16)$$

where E_{JT} is the Jahn−Teller stabilization energy and ω is the vibrational frequencies, the vibrational mode of which couple to the degenerate electronic state.[32] If magnitude of S is infinite ("strong coupling" or "classical limit"), the zero-point vibration can be ignored. On the other hand, at small S quantum effect becomes important.

The E_{JT} are tabulated in Table 8. On the other hand, the vibrational energies of the JT-active modes fall in the range of 0.02−0.37 eV. Therefore S is of order of 1−10, which means that the JT coupling is comparable to or larger than the zero-point vibrational energies. Janata et al. have observed ten equivalent hydrogens from the hyperfine structures of ESR spectrum of monoanion at room temperature.[14] This can be interpreted as five equivalent symmetry-lowered configurations with C_s symmetry of monoanion undergo dynamical interconversion at room temperature. In other words, dynamic JT effect occurs in corannulene monoanion. JT distorted structures of these anionic states may be observed in the low temperature.

TABLE 6: Atomic Net Charge of Corannulene and Its Anions Calculated at the MP2/6-31G//HF/6-31G** Level**

	1	$\mathbf{1}^-$	$\mathbf{1}^{2-}$
hub	−0.047856	−0.04759 to −0.095 20	−0.07319 to −0.140 01
flank	0.046281	0.02974 to 0.080 57	0.06783 to 0.073 40
rim	−0.121779	−0.12813 to −0.198 90	−0.13707 to −0.216 05
protons	0.122566	0.06054 to 0.083 54	−0.01416 to 0.013 79

	$\mathbf{1}^{3-}$	$\mathbf{1}^{4-}$
hub	−0.11756 to −0.15967	−0.13795 to −0.16924
flank	0.08388 to 0.15403	0.10164 to 0.10865
rim	−0.17688 to −0.30428	−0.20339 to −0.28625
protons	−0.04879 to −0.09137	−0.12858 to −0.14157

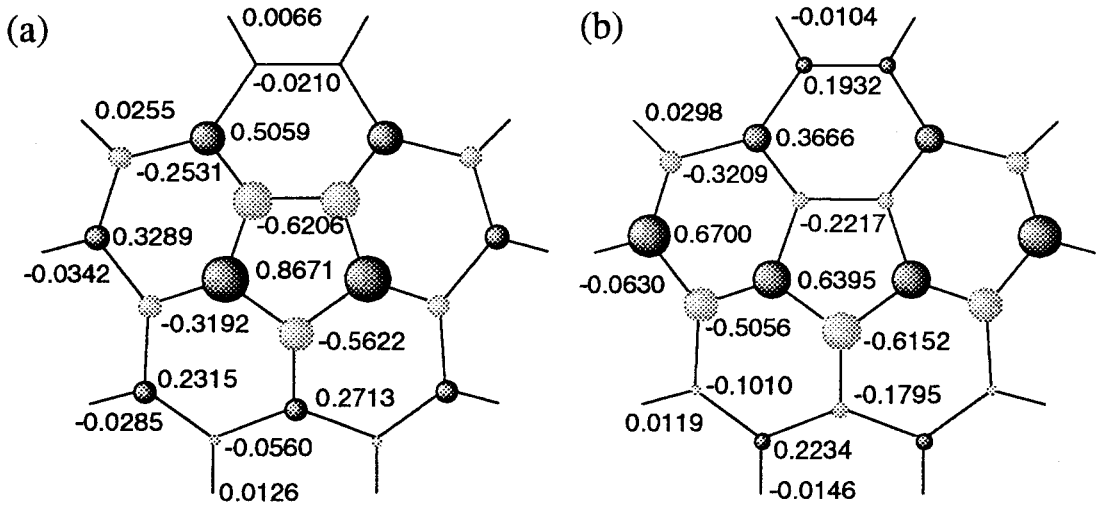

Figure 4. The spin densities of (a)$\mathbf{1}^-$ and (b) $\mathbf{1}^{3-}$ calculated with MP2/6-31G**//HF/6-31G** method. The black circle in this figures mean the excess of α spin.

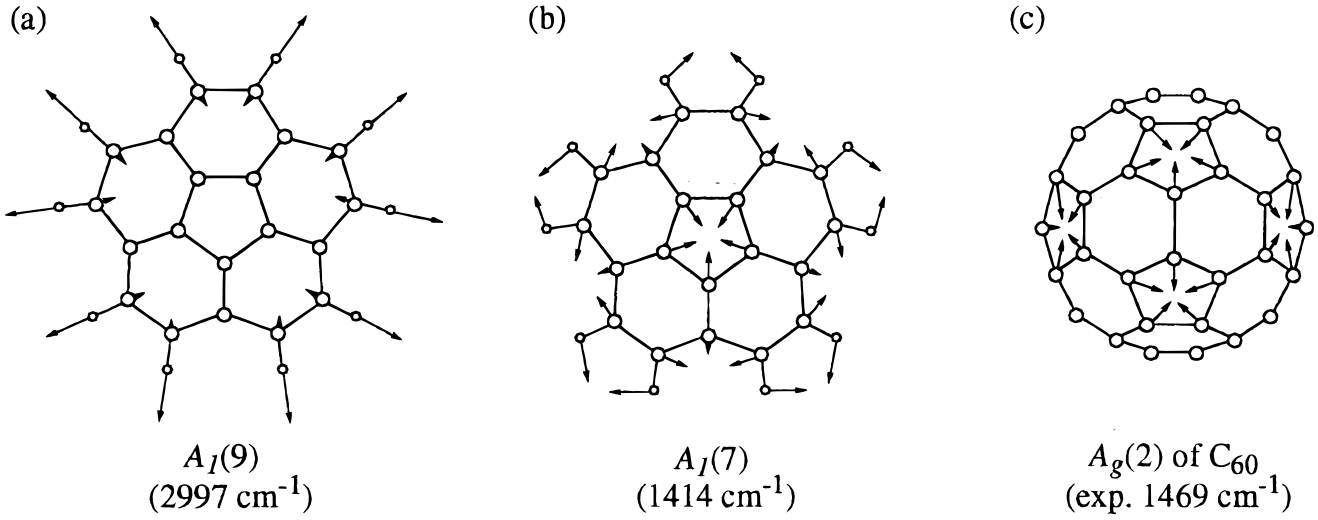

Figure 5. Two of the most intensive Raman-active A_1 modes of **1** (a) $A_1(9)$, (b) $A_1(7)$, and (c) pentagonal pinch mode $A_g(2)$ of C_{60}.

As shown in Table 8, the magnitude of E_{JT} of $\mathbf{1}^{3-}$ is 2 or 3 times larger than that of $\mathbf{1}^-$.

Comparing them with E_{JT} of C_{60}^-, ca. 0.04 eV,[33,34] JT stabilization energy in the present systems is larger than that of C_{60}^-.

4. Conclusion

The electronic and vibrational structures of $\mathbf{1}^{n-}$ ($n = 0$, 1, 2, 3, and 4) was studied on the basis of the ab initio MO calculation at HF/6-31G** level, and we also studied the electronic structure of corannulene anions based on the single-point post HF calculation at MP2/6-31G**//HF/6-31G** and CASSCF/6-31G**//HF/6-31G** level of theory. The major findings for corannulene and its anions through the present study are as follows: (1) In each structure of corannulene anion studied here there occurs symmetry lowering from C_{5v} into C_s due to the Jahn−Teller effect for $\mathbf{1}^{1-}$ and $\mathbf{1}^{3-}$ or to the pseudo-Jahn−Teller effect for $\mathbf{1}^{2-}$ and $\mathbf{1}^{4-}$. (2) The bowl-shaped structure of corannulene becomes flatter when it becomes anionic. (3) The wavenumber of IR-active C−H stretching mode give rise to red shift with reduction. We suggest that this absorption can be used as an identification of the reduction state of a corannulene anion. (4) The ground state of the monoanion and the trianion are both $^2A'$ state in the HF levels of theory. (5) The ground

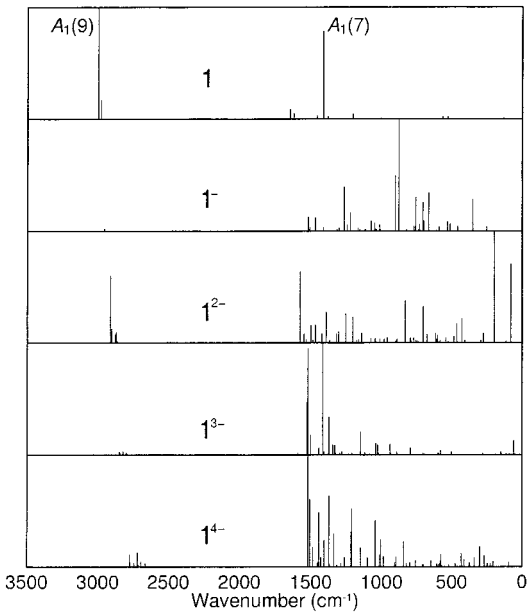

Figure 6. Simulated Raman spectra of the ground states of corannulene anions based on vibration analyses. The vibrational modes of $A_1(9)$ and $A_1(7)$ are shown in Figure 5.

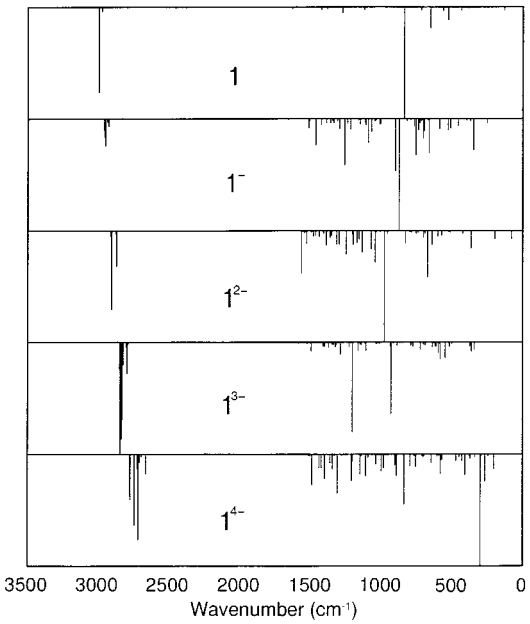

Figure 7. Simulated IR absorption spectra of the ground states of corannulene anions based on vibration analyses.

TABLE 7: Vibrational Frequencies of A_1 and E_2 Modes, IR Intensities, and Raman Activities of 1 Calculated Using RHF/6-31G**

species	frequencies	IR intensities	Raman activities
$A_1(1)$	133	5.5013	9.3689
$A_1(2)$	534	17.5242	21.1719
$A_1(3)$	570	5.2284	21.5908
$A_1(4)$	845	146.9843	2.4028
$A_1(5)$	1002	1.3731	7.9603
$A_1(6)$	1205	1.1284	41.3214
$A_1(7)$	1414	1.4915	694.6447
$A_1(8)$	1623	0.0000	44.4823
$A_1(9)$	2997	6.2566	888.0625
$E_2(1)$	137	0.0000	3.1805
$E_2(2)$	272	0.0000	1.9600
$E_2(3)$	419	0.0000	6.1443
$E_2(4)$	524	0.0000	2.4612
$E_2(5)$	588	0.0000	0.0658
$E_2(6)$	622	0.0000	0.5562
$E_2(7)$	759	0.0000	0.2406
$E_2(8)$	793	0.0000	0.0744
$E_2(9)$	984	0.0000	0.1754
$E_2(10)$	1022	0.0000	2.7153
$E_2(11)$	1095	0.0000	3.9707
$E_2(12)$	1126	0.0000	9.0091
$E_2(13)$	1328	0.0000	4.2131
$E_2(14)$	1382	0.0000	22.5250
$E_2(15)$	1455	0.0000	25.5307
$E_2(16)$	1648	0.0000	82.0643
$E_2(17)$	2977	0.0000	151.0909
$E_2(18)$	2994	0.0000	161.3406

state of the dianion is a singlet, which is consistent with the experimental result in all the levels of theory employed here. (6) The Jahn−Teller stabilization energy of the trianion is larger than that of monoanion. The monoanion seems to be a dynamic Jahn−Teller system. Furthermore the stabilization energies are larger than that of C_{60}. Experimental study on observation of JT effect in these anions is now in progress. The results will be published elsewhere in the near future.

Acknowledgment. T.S. and A.Y. thank Professor K. Tanaka of this department for valuable discussions. This work was supported by a Grant-in-Aid for Scientific Research from the Ministry of Education, Science, and Culture of Japan. Numerical calculations were carried out at the Super Computer Laboratory, Institute for Chemical Research, Kyoto University and the Kyoto University Data Processing Center. This work was also supported by the Research for the Future Program from the Japan Society for the Promotion of Science (Grant JSPS-RFTF96-P00206).

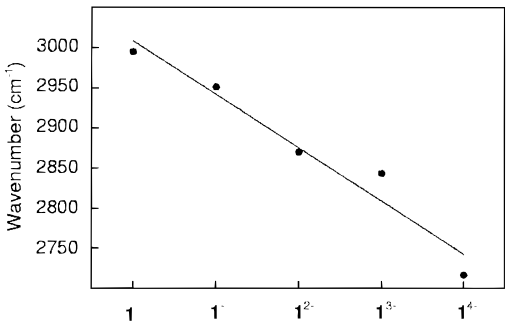

Figure 8. Relation between the reduction state of corannulene and the wavenumber of C−H stretching mode.

TABLE 8: Jahn−Teller Stabilization Energies ($E_{JT} = E_{C5v} - E_{Cs}$, in eV) of 1^- and 1^{3-}

	HF/6-31G**	MP2/6-31G**//HF/6-31G**
$\mathbf{1}^-$	0.313240	0.494175
$\mathbf{1}^{3-}$	0.907828	1.171899

References and Notes

(1) Barth, W.; Lawton, R. *J. Am. Chem. Soc.* **1966**, *88*, 380.
(2) Barth, W.; Lawton, R. *J. Am. Chem. Soc.* **1971**, *93*, 1730.
(3) Gleicher, G. *Tetrahedron* **1967**, *23*, 4257.
(4) Hanson, J.; Nordman, C. *Acta Crystallogr.* **1976**, *B32*, 1147.
(5) Osawa, E. *Kagaku (Chemistry)* **1970**, *25*, 850 (in Japanese).
(6) Kroto, H.; Heath, J.; O'Brien, S.; Curl, R.; Smalley, R. *Nature* **1985**, *318*, 162.
(7) Scott, L.; Hashemi, M.; Meyer, D.; Warren, H. *J. Am. Chem. Soc.* **1991**, *113*, 7082.
(8) Borchardt, A.; Fuchicello, A.; Kilway, K.; Baldridge, K.; Siegel, J. *J. Am. Chem. Soc.* **1992**, *114*, 1921.
(9) Scott, L.; Cheng, P.-C.; Hashemi, M.; Bratcher, M.; Meyer, D.; Warren, H. *J. Am. Chem. Soc.* **1997**, *119*, 10963.
(10) Wynberg, H.; Nieuwpoort, W.; Jonkman, H. *Tetrahedron Letters* **1973**, *46*, 4623.
(11) Scott, L.; Hashemi, M.; Bratcher, M. *J. Am. Chem. Soc.* **1992**, *114*, 1920.
(12) Ayalon, A.; Rabinovitz, M.; Cheng, P.-C.; Scott, L. *Angew. Chem., Int. Ed. Engl.* **1992**, *31*, 1636.
(13) Cyvin, S.; Brendsdal, E.; Brunvoll, J.; Skaret, M. *J. Mol. Struct.* **1991**, *247*, 119.
(14) Janata, J.; Gendell, J.; Ling, C.-Y.; Barth, W.; Backes, L.; H. B. Mark, J.; Lawton, R. *J. Am. Chem. Soc.* **1967**, *89*, 3056.
(15) Baumgarten, M.; Gherghel, L.; Wagner, M.; Weitz, A.; Rabinovitz, M.; Cheng, P.-C.; Scott, L. *J. Am. Chem. Soc.* **1995**, *117*, 6254.
(16) Ayalon, A.; Sygula, A.; Cheng, P.-C.; Rabinovitz, M.; Rabideau, P.; Scott, L. *Science* **1994**, *265*, 1065.
(17) Kiyobayashi, T.; Nagano, Y.; Sakiyama, M.; Yamamoto, K.; Cheng, P.-C.; Scott, L. *J. Am. Chem. Soc.* **1995**, *117*, 3270.
(18) Schulman, J.; Peck, R.; Disch, R. *J. Am. Chem. Soc.* **1989**, *111*, 5675.
(19) Tanaka, K.; Sato, T.; Okada, M.; Yamabe, T. *Fullerene Sci. Technol.* **1996**, *4*, 863.
(20) Sygula, A.; Rabideau, P. *J. Mol. Struct. (Theochem)* **1995**, *333*, 215.
(21) Disch, R.; Schulman, J. *J. Am. Chem. Soc.* **1994**, *116*, 1533.
(22) Tanaka, K.; Okada, M.; Okahara, K.; Yamabe, T. *Chem. Phys. Lett.* **1992**, *193*, 101.
(23) Koga, N.; Morokuma, K. *Chem. Phys. Lett.* **1992**, *196*, 191.
(24) Jahn, H.; Teller, E. *Proc. R. Soc. London, Ser. A* **1937**, *161*, 220.
(25) Radom, L. In *Application of Electronic Structure Theory*, Schaefer, H. F., III, Ed.; Plenum Press: New York, 1977; Chapter 8, pp 333−356.
(26) Pople, J. In *Applications of Electronic Structure Theory*, Plenum Press: New York, 1977; Chapter 1, pp 1−27.
(27) Frisch, M. J.; Trucks, G. W.; Schlegel, H. B.; Gill, P. M. W.; Johnson, B. G.; Robb, M. A.; Cheeseman, J. R.; Keith, T.; Petersson, G. A.; Montgomery, J. A.; Raghavachari, K.; Al-Laham, M. A.; Zakrzewski,

V. G.; Ortiz, J. V.; Foresman, J. B.; Cioslowski, J.; Stefanov, B. B.; Nanayakkara, A.; Challacombe, M.; Peng, C. Y.; Ayala, P. Y.; Chen, W.; Wong, M. W.; Andres, J. L.; Replogle, E. S.; Gomperts, R.; Martin, R. L.; Fox, D. J.; Binkley, J. S.; Defrees, D. J.; Baker, J.; Stewart, J. P.; Head-Gordon, M.; Gonzalez, C.; Pople, J. A. *Gaussian 94*, Revision D.3; Gaussian, Inc: Pittsburgh, PA, 1995.

(28) Frisch, M. J.; Frisch, M. J.; Trucks, G. W.; Schlegel, H. B.; Scuseria, G. E.; Robb, M. A.; Cheeseman, J. R.; Zakrzewski, V. G.; J. A. Montgomery, J.; Stratmann, R. E.; Burant, J. C.; Dapprich, S.; Millam, J. M.; Daniels, A. D.; Kudin, K. N.; Strain, M. C.; Farkas, O.; Tomasi, J.; Barone, V.; Cossi, M.; Cammi, R.; Mennucci, B.; Pomelli, C.; Adamo, C.; Clifford, S.; Ochterski, J.; Petersson, G. A.; Ayala, P. Y.; Cui, Q.; Morokuma, K.; Malick, D. K.; Rabuck, A. D.; Raghavachari, K.; Foresman, J. B.; Cioslowski, J.; Ortiz, J. V.; Stefanov, B. B.; Liu, G.; Liashenko, A.; Piskorz, P.; Komaromi, I.; Gomperts, R.; Martin, R. L.; Fox, D. J.; Keith, T.; Al-Laham, M. A.; Peng, C. Y.; Nanayakkara, A.; Gonzalez, C.; Challacombe, M.; Gill, P. M. W.; Johnson, B.; Chen, W.; Wong, M. W.; Andres, J. L.; Gonzalez, C.; Head-Gordon, M.; Replogle, E. S.; Pople, J. A. *Gaussian 98*, Revision A.5; Gaussian, Inc.: Pittsburgh, PA, 1998.

(29) Pople, J.; Schlegel, H.; Krishnan, R.; Defrees, D.; Binkley, J.; Frisch, M.; Whiteside, R.; Hout, R.; Hehre, W. *Int. J. Quantum Chem. Symp.* **1981**, *15*, 269.

(30) Mitch, M.; Lannin, J. *Phys. Rev. B* **1995**, *51*, 6784.

(31) Dresselhaus, M. S.; Dresselhaus, G.; Eklund, P. *Science of Fullerenes and Carbon Nanotubes*; Academic Press: New York, 1996.

(32) O'Brien, M. *J. Phys. C: Solid State Phys.* **1971**, *4*, 2524.

(33) Varma, C.; Zaanen, J.; Raghavachari, K. *Science* **1991**, *254*, 989.

(34) Schluter, M.; Lanoo, M.; Needles, M.; Baraff, G.; Tomanek, D. *Phys. Rev. Lett.* **1991**, *68*, 526.